# Using the estimated velocity of seismic waves from ambient seismic noise to assess the results of hydro-fracturing and the exploitation of shale-rock formations

**Henryk Marcak[1], Janusz Mirek[1], Mateusz Lasak[1]**

hmarcak@igf.edu.pl, jmirek@igf.edu.pl, mlasak@igf.edu.pl

[1] Institute of Geophysics, Polish Academy of Sciences, Warszawa, Poland

Institute of Geophysics
Polish Academy of Sciences

24 April 2017, Vienna

# Seismic interferometry ⇔Hydro-fracturing

**Henryk Marcak[1], Janusz Mirek[1], Mateusz Lasak[1]**

hmarcak@igf.edu.pl, jmirek@igf.edu.pl, mlasak@igf.edu.pl

[1] Institute of Geophysics, Polish Academy of Sciences, Warszawa, Poland

Institute of Geophysics
Polish Academy of Sciences

24 April 2017, Vienna

# Research problems / Subjects of investigation

**1.** Can we get information from just one source (one station)?

**YES!** (using cross-correlation of horizontal components of seismic noise)

**2.** Can we measure the velocity changes at the depth of 4000 m?

**YES!** (using stretching parameter)

Institute of Geophysics
Polish Academy of Sciences

# Fundamentals of seismic interferometry

The basic equation of  of 1D direct-wave seismic interferometry has the following form (Wapenaar et al. 2010):

$$G(x_B, x_A, t)S(t) = u(x_B, x_s, t) * u(x_A, x_s, -t)$$

where

$u(x_B, x_s, t)$ is the seismic response (in point $x_B$) to signals coming from the source $x_s$ at time t,

$x_A$ *and* $x_B$ are the positions of the receivers,

$x_s$ is the position of the source,

$S(t)$ is the autocorrelation of the wavelet,

$G(x_B, x_A, t)$ is the Green function for the signal recorded in $x_B$ with source in $x_A$, and

$u(x_B, x_s, t) * u(x_A, t_0, -t)$ is the convolution of $u(x_B, x_s, t)$ and $(x_A, x_s, -t)$ functions.

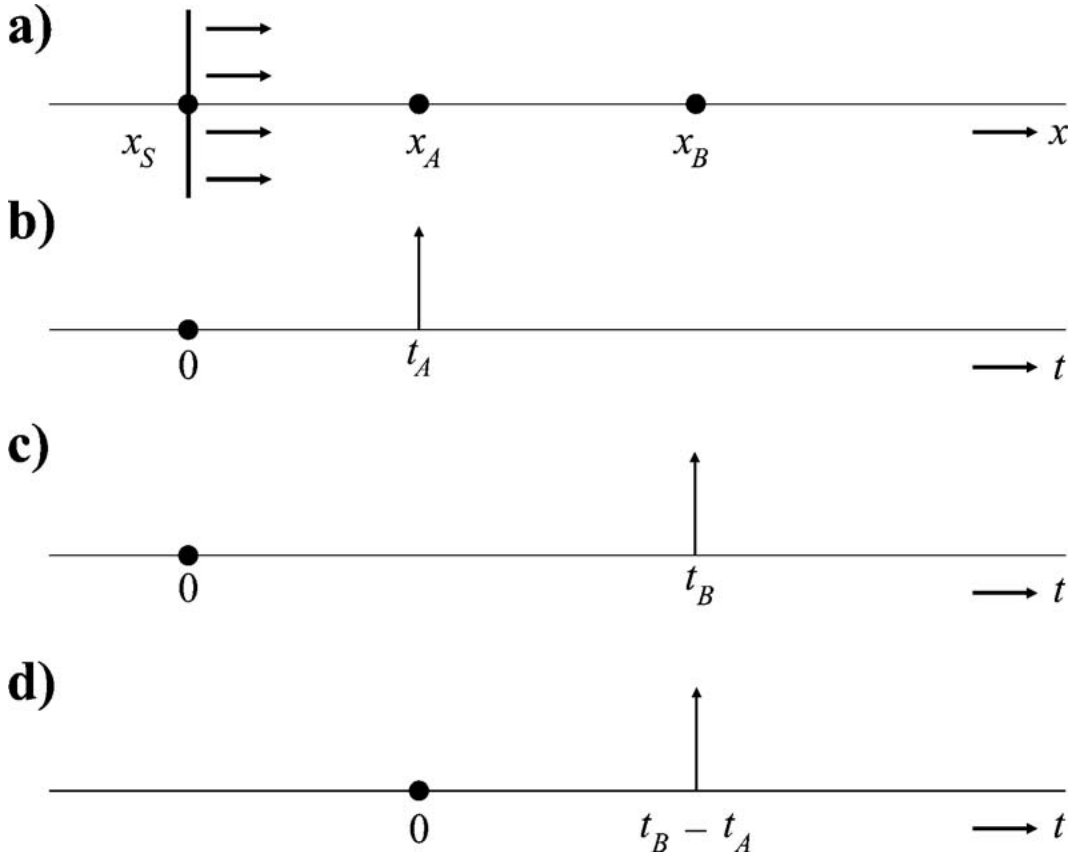


**Fig. 1** A 1D example of direct-wave interferometry (Wapenaar et al. 2010).

# Hydro-fracturing ⇔ Seismic interferometry

2 different regimes connected with hydro-fracturing are particularly interesting and could be investigated by seismic interferometry methods (Obermann et al. 2013):

- **shallow zone** (usual location of water aquifer)
  - the best sensitivity for discriminating shallow perturbations of seismic velocities can be researched with fundamental modes of **surface waves**,

- **deep zone** (parts of rock masses situated near fracked intervals of the borehole – earthquakes are usually located within this zone) – **coda waves**

- surface waves dominate the depth sensitivity at shallow depths and at early times in the coda.
- bulk waves dominate the depth sensitivity at greater depths and at later times in the coda.

# Seismic network

http://www.sheerproject.eu/

| Hydro-fracturing time-table | | |
|---|---|---|
| | Wysin-2-H & Wysin 2-H' | Wysin 3-H |
| **Date of hydro-fracturing** | 08.06.2016 - 18.06.2016 | 19.07.2016 - 29.07.016 |
| **Number of hydro-fractured intervals** | 11 stages | 11 stages |

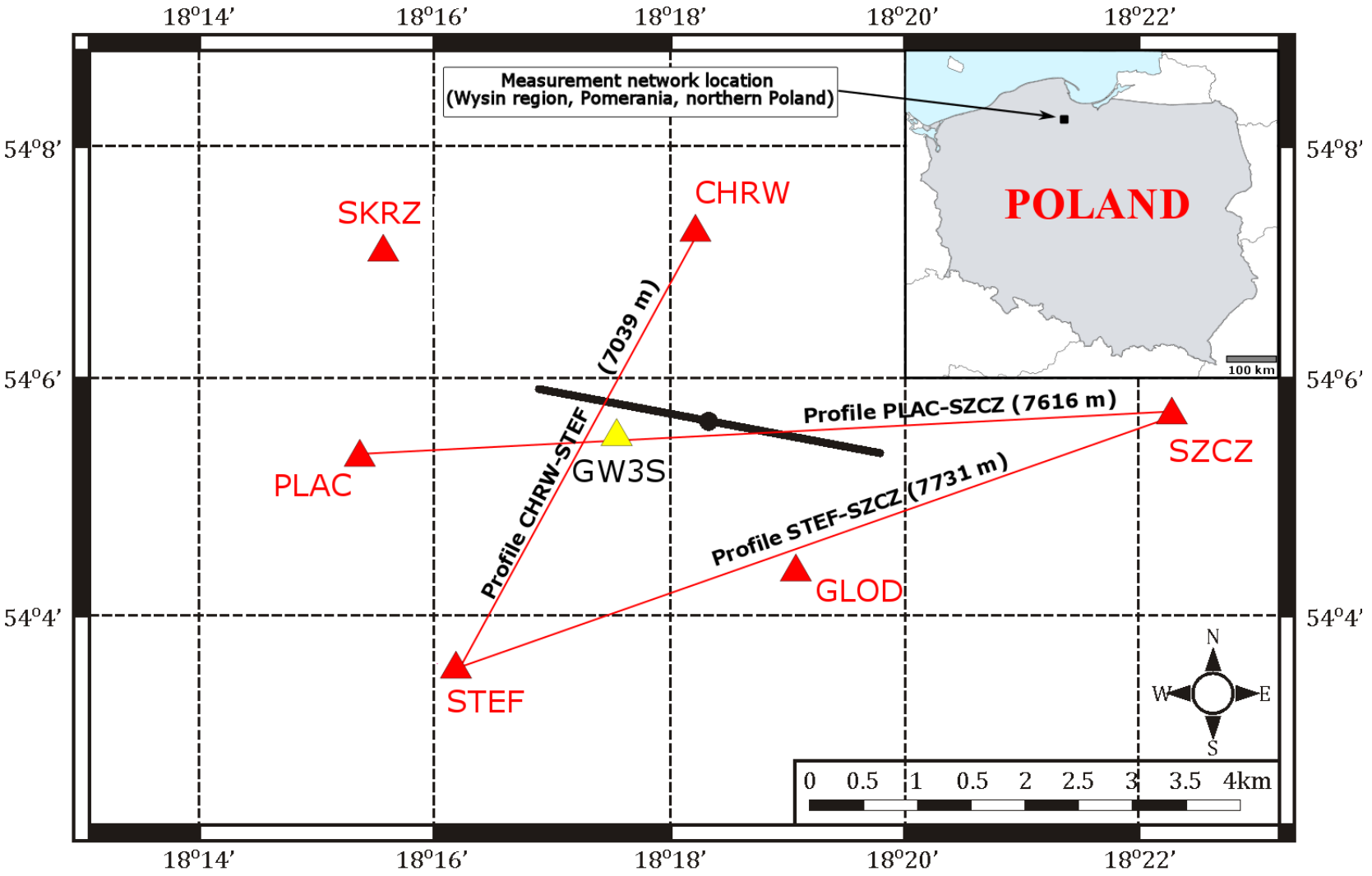


**Fig. 2** The location of broad-band seismometers in the area surrounding the Wysin-2-H and Wysin 3-H wells.

- Wysin-2-H and Wysin-3-H wells with horizontal sections
- unit in shallow borehole
- surface units

Institute of Geophysics
Polish Academy of Sciences

# Geology

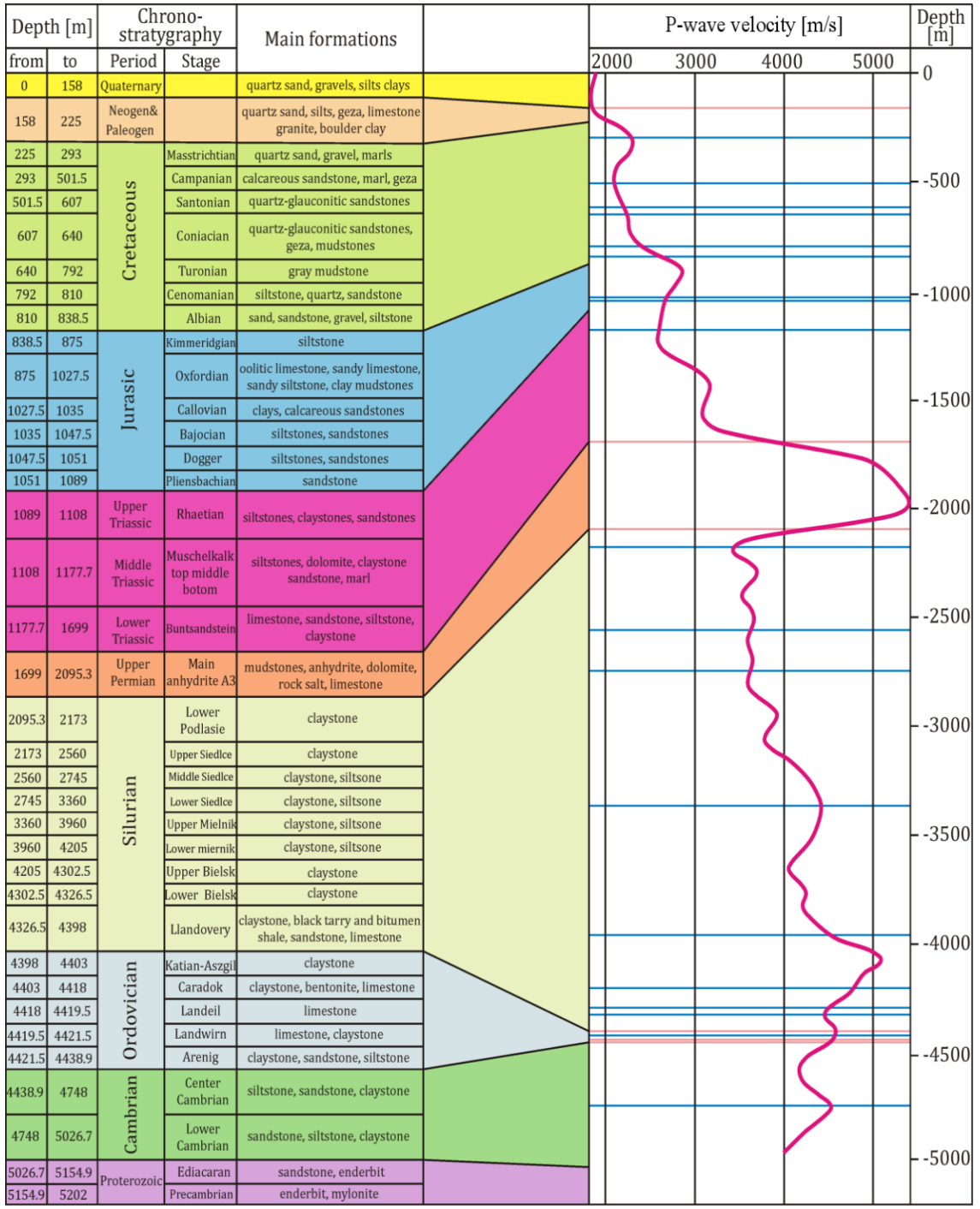


**Fig. 3** A geological cross-section of the Wysin region.

**Thick post-glacial cover (0 - 200 m)**

**Anhydrite (1700 - 2100 m)**

P-wave velocity almost 2 km/s higher than surrounding formations

**Target shale formations (located within interval: 3700 - 4000 m)**

Lower Silurian (Wenlok)

Institute of Geophysics
Polish Academy of Sciences

# Coda waves

Difficulties in coda waves registration:

- **strong seismic reflector - Permian Anhydrites (1700 – 2100 m)** - coda waves are reflected upwards and do not reach the depth interval of target formations
- **200-m thick post-glacial cover** - dispersion of the reflected waves.

Cross-correlations of horizontal components of seismic noise recored at one station:

- have signals at lapse time τ range, in which scattered coda waves can be present,
- these waves seem to be transmitted vertically => can penetrate deep even in a geologically complicated medium
- observable changes of cross-correlations for both positive and negative sides of correlogram => posibble occurrence of split waves (shear waves after splitting due to anisotropic medium to slower and faster split waves)

# Stretching coefficient

Distinguishing the CCFs obtained in the periods before, during and after fracking requires:

- **a longer observation time,**
- **location of the seismic station directly over the hydro-fracktured borehole.**

The parameter $\varepsilon_{max}$ was estimated by maximizing the correlation coefficient between the two waveforms in the selected time window: (Hadziioannou et al. 2009):

$$CC(\varepsilon) = \frac{\int_{t_1}^{t_2} f_{tem}(t(1-\varepsilon) f_{ref}(t) dt}{\sqrt{\int_{t_1}^{t_2} (f_{tem}(t(1-\varepsilon))^2 dt} \sqrt{\int_{t_1}^{t_2} (f_{ref}(t))^2 dt}}$$

where

$f_{tem}$ is the current cross-correlation function CCF in the time window $[t_1, t_2]$,

$f_{ref}$ is the average cross-correlation function; reference trace.

# Estimation of the fracking effects for shallow borehole station (GW3S)

| Reference trace | Standard deviation for ref. trace [s] | Data trace | Standard deviation for data trace [s] | Stretching parameter $\varepsilon_{max}$ [s] | Correlation coefficient $CC(\varepsilon)$ |
|---|---|---|---|---|---|
| 1st Period | 0.0022 | 2nd Period | 0.0023 | -0,0090 | 0.96 |
| 1st Period | 0.0022 | 3rd Period | 0.0035 | -0,0090 | 0.96 |
| 1st Period | 0.0022 | 4th Period | 0.0019 | -0,0005 | 0.96 |
| 2nd Period | 0.0023 | 3rd Period | 0.0035 | 0 | 0.99 |
| 2nd Period | 0.0023 | 4th Period | 0.0019 | 0,0080 | 0.97 |
| 3rd Period | 0.0035 | 4th Period | 0.0019 | 0,0080 | 0.97 |

**Tab. 1** The estimates of the stretching parameters between mean CCF calculated from data recorded by GW3S station in the different time periods:

- 1st period: 1.05.2016 – 07.06.2016 (before hydrofracturing)
- 2nd period: 18.06.2016 – 18.07.2016 (after fracking of the Wysin-2-H/ Wysin-2-H')
- 3rd period: 29.07.2016 – 31.08.2016 (after fracking of the Wysin-3-H)
- 4th period: 01.09.2016 – 31.10.2016 (period month after last stage of fracking occurred).

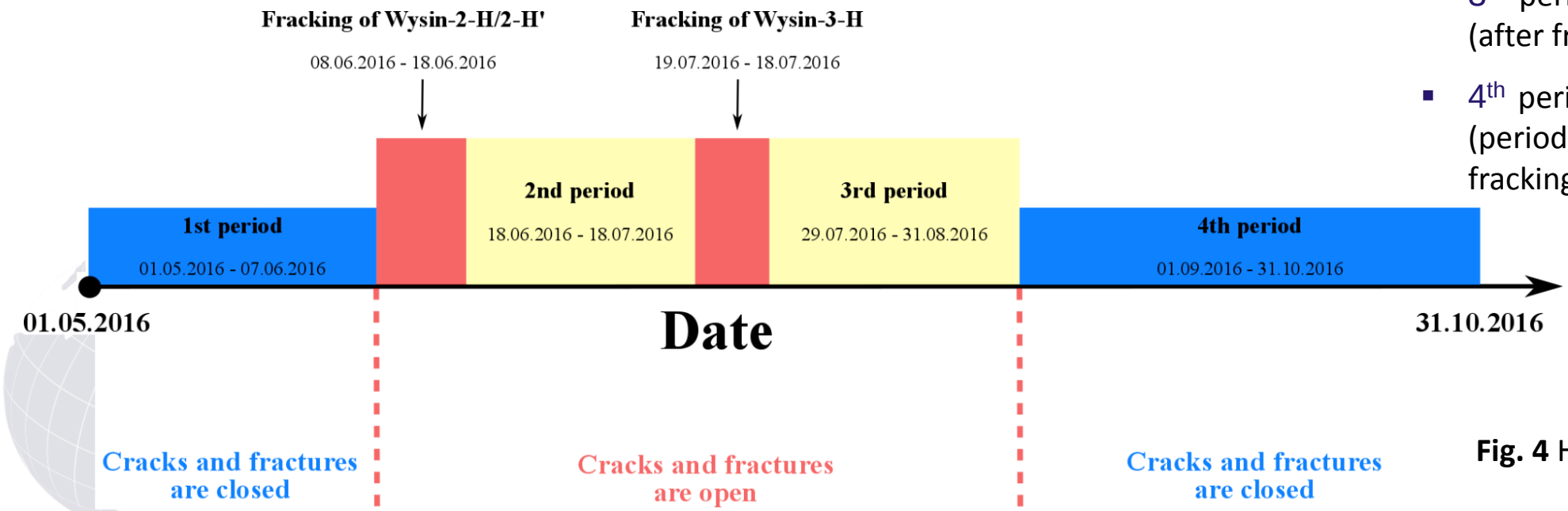


**Fig. 4** Hydro-fracturing time-table

# Influence of the movement of the source noise on the CCF shape

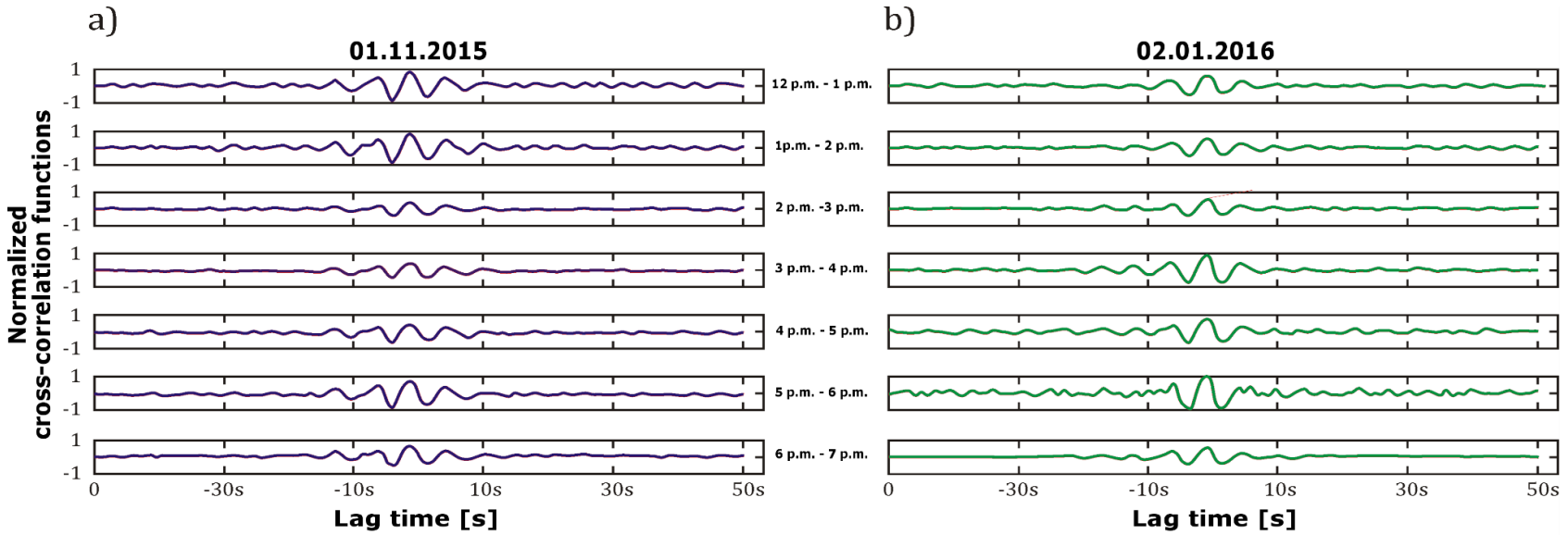


**Fig. 5** Correlograms calculated from 1-hour noise records from: 01.11.2015 (**Fig. 5a**), 02.01.2016 (**Fig. 5b**), for PLAC-CHRW profile; average CCF functions for both days (**Fig. 5c**).

CCF functions were calculated, then filtered by frequency band 0 - 1 Hz, and average CCF functions for both days were computed.

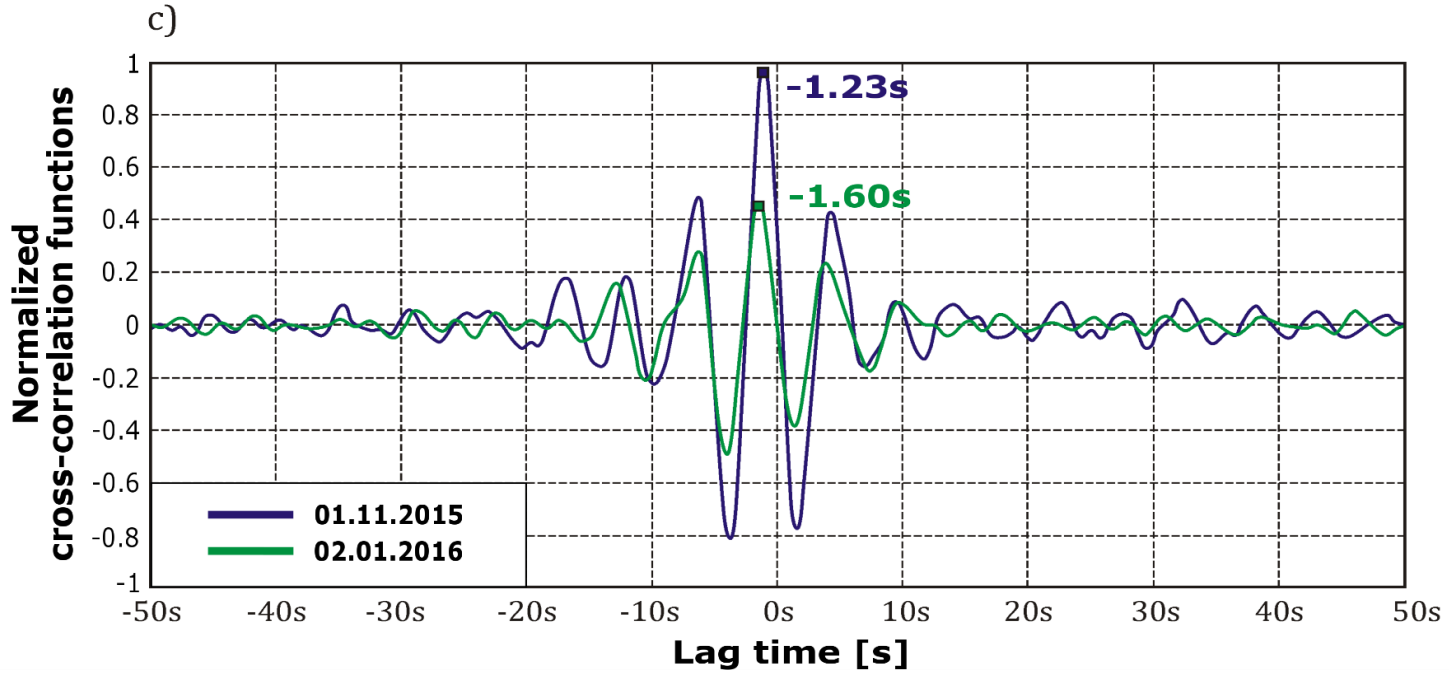


Institute of Geophysics
Polish Academy of Sciences

# Influence of the movement of the external source noise on the CCF shape

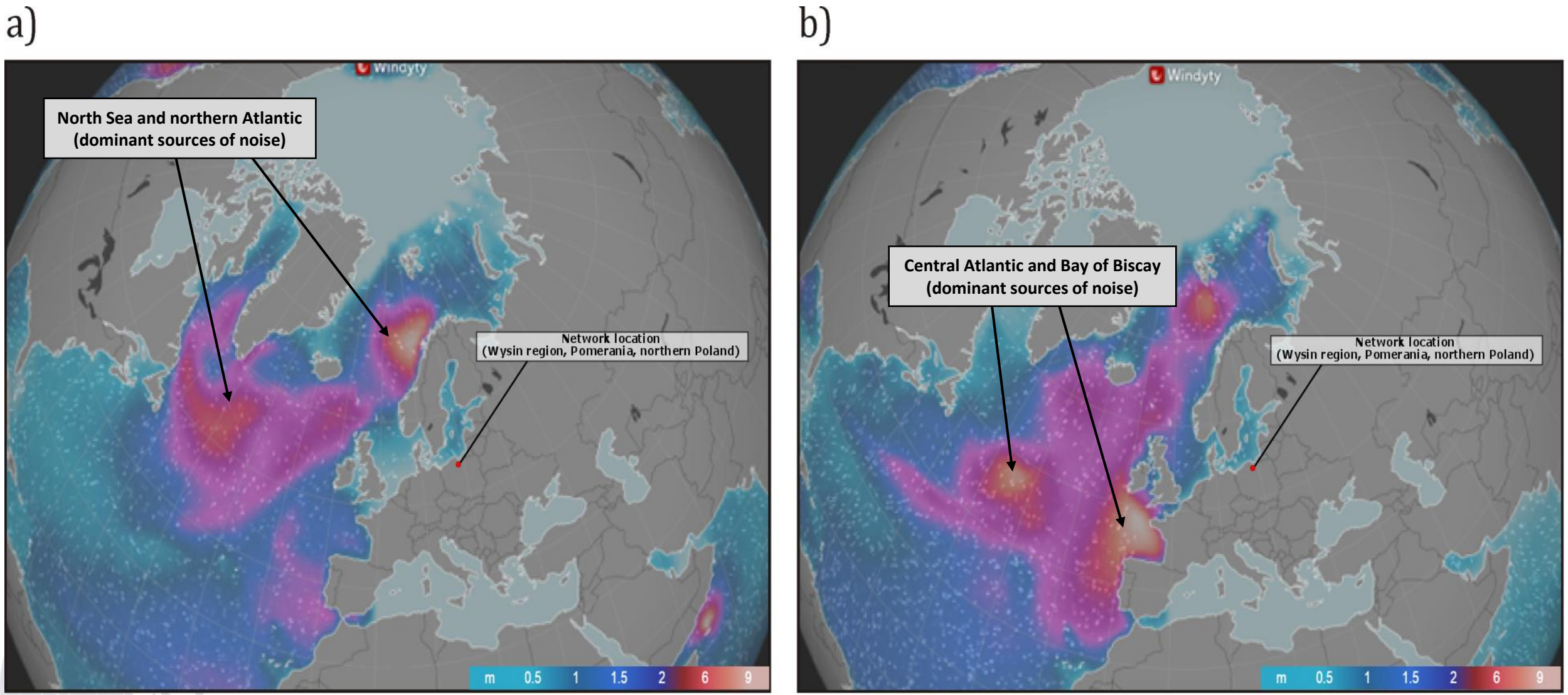


**Fig. 6** Sea waving intensity on 01.11.2015 (Fig. 5a) and 02.01.2016 (Fig. 5b) (source: https://www.windytv.com/).

**Fig. 7** Dispersion diagram after Δt time shifting on the CHRW-STEF profile (**Fig. 7a**).

Dispersion diagram after Δt time shifting on the PLAC-SZCZ profile (**Fig. 7b**);

Fundamental mode of the Rayleigh waves for the PLAC-SZCZ profile (**Fig. 7c**, colour scale - misfit value).

The set of solutions and corresponding 1-dimensional dispersion curves for different misfit parameters for the PLAC-SZCZ profile (**Fig. 7d**, colour scale – misfit value).

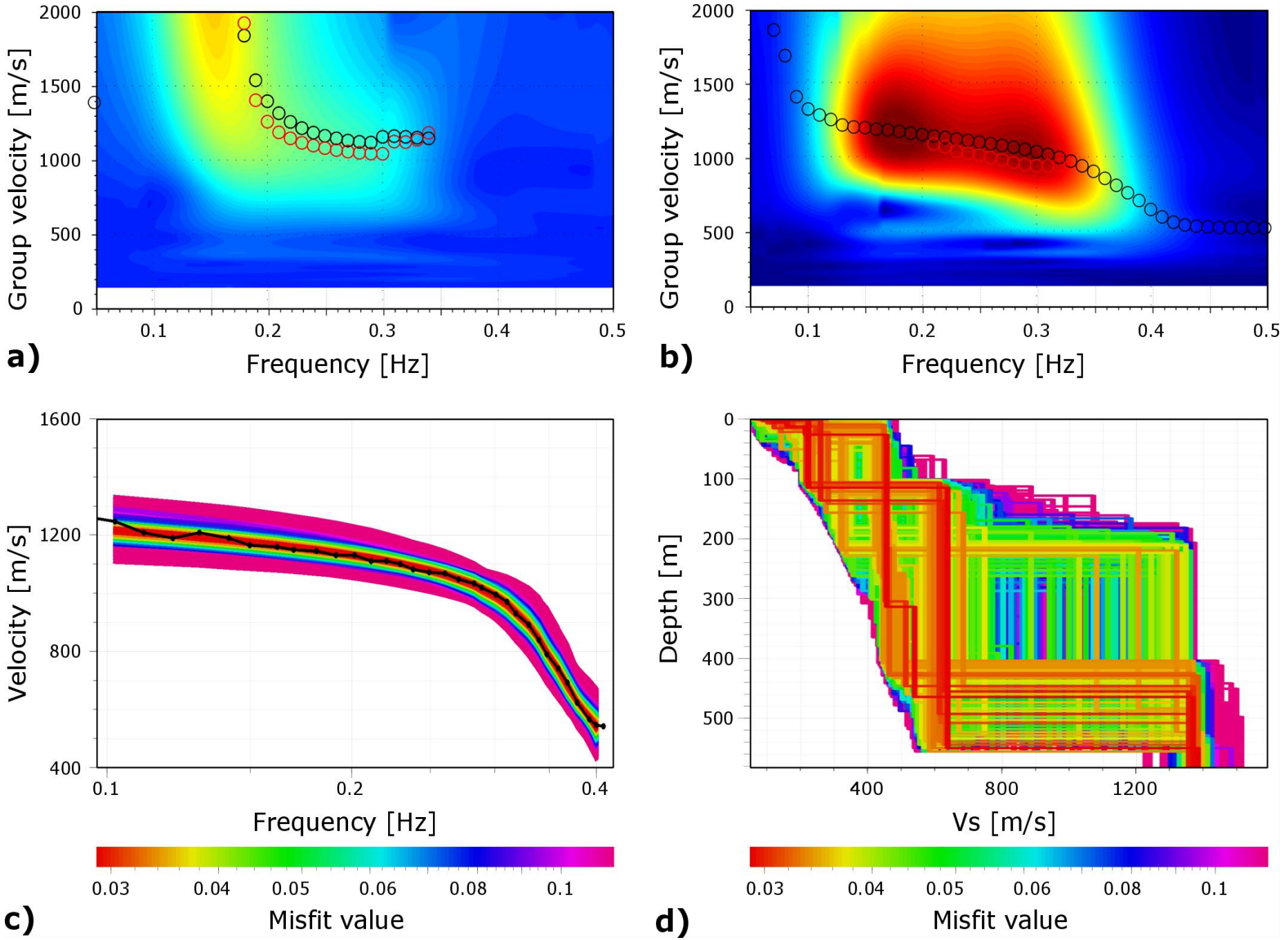

# Conclusions

**1.** Can we get information from just one source (one station)?

**YES!** CCF of horizontal components have scattered signals in coda window => vertical propagation => large depth range (even to the depth of shale gas deposits!)

**2.** Can we measure the velocity changes at the depth of 4000 m?

**YES!** Calculations of stretching parameter indicate large differences between periods when cracks and fractures were closed and periods when cracks and fractures were open => velocity changes!

# References

Selected positions:


- Bensen G. D., Ritzwoller M. H., Barmin M. P., Levshin A. L., Lin F., Moschetti M. P., Shapiro N. M., Yang Y. (2007). Processing seismic ambient noise data to obtain reliable broad-band surface wave dispersion measurements. *Geophys. J. Int.*, 169 (3), 1239-1260, doi: 10.1111/j.1365-246X.2007.03374.x
- Campillo, M., Paul A. (2003). Long-range correlations in the diffuse seismic coda. *Science*, 299 (5606), 547-549, doi: 10.1126/science.1078551
- Curtis A., Gerstoft P., Sato H., Snieder R., Wapenaar K. (2006). Seismic interferometry - turning noise into signal. The Leading Edge. 25 (9), 1082-1092, doi: 10.1190/1.2349814
- Czarny R., Marcak H., Nakata N., Pilecki Z., Isakow Z. (2016). Monitoring Velocity Changes Caused By Underground Coal Mining Using Seismic Noise. *Pure and Applied Geophysics*, 173 (6), 1907-1916, doi: 10.1007/s00024-015-1234-3
- Hadziioannou, C., Larose E., Coutant O., Roux P., Campillo M. (2009). Stability of monitoring weak changes in multiply scattering media with ambient noise correlation: laboratory experiments., *J. Acoust. Soc. Am*., 125 (6), 3688–3695, doi: 10.1121/ 1.3125345
- Halliday D., Curtis A. (2008). Seismic interferometry, surface waves and source distribution. *Geophys. J. Int.* 175, 1067-1087, doi: 10.1111/j.1365-246X.2008.03918.x
- Hillers G., Husen S., Obermann A., Planès T., Larose E., Campillo M. (2015). Noise-based monitoring and imaging of aseismic transient deformation induced by the 2006 Basel reservoir stimulation. *Geophysics*, 80 (4), doi: 10.1190/geo2014-0455.1
- Jurkevics A. (1988). Polarization analysis of three-component array data. *Bulletin of the Seismological Society of America*, 78(5), 1725-1743
- Kedar S., Longuet-Higgins M., Webb F., Graham N., Clayton R., Jones C. (2008). The origin of deep ocean microseisms in the North Atlantic Ocean. *Proc. R. Soc. A*, 464 (2091) 777-793, doi: 10.1098/rspa.2007.0277
- Obermann A., Planès T., Larose E., Sens-Schönfelder C., Campillo M. (2013). Depth sensitivity of seismic code waves to velocity perturbation in an elastic heterogeneous medium. *Geoph. J. Int.*, 194, 372-382, doi: 10.1093/gji/ggt043
- Shapiro N. M., Campillo M. (2004). Emergence of broadband Rayleigh waves from correlations of the ambient seismic noise. *Geophys. Res. Lett.*, 31 (7), doi: 10.1029/2004GL019491
- Silver P. G., Chan W. W. (1991). Shear wave splitting and subcontinental mantle deformation. J. Geoph. Res., doi: 10.1029/91JB00899
- Snieder R. (2004). Extracting the Green's function from the correlation of coda waves: A derivation based on stationary phase. *Phys. Rev. E*, 93, 046610, doi: 10.1103/PhysRevE.69.046610
- Snieder R. (2006). The theory of coda wave interferometry. *Pure and Applied Geophysics*, 163, 455-473, doi: 10.1007/s00024-005-0026-6
- Wapenaar K., Draganov D., Snieder R., Campman X., Verdel A. (2010). Tutorial on seismic interferometry: Part 1 — Basic principles and applications. Geophysics, 75, 75A195–75A209, doi: 10.1190/1.3457445

# Thank you
# for your attention!

Acknowledgements:
This work was supported under SHEER: "Shale Gas Exploration and Exploitation Induced Risks" project funded from Horizon 2020 – R&I Framework Programme, call H2020-LCE-2014-1.

Institute of Geophysics
Polish Academy of Sciences

# Additional information

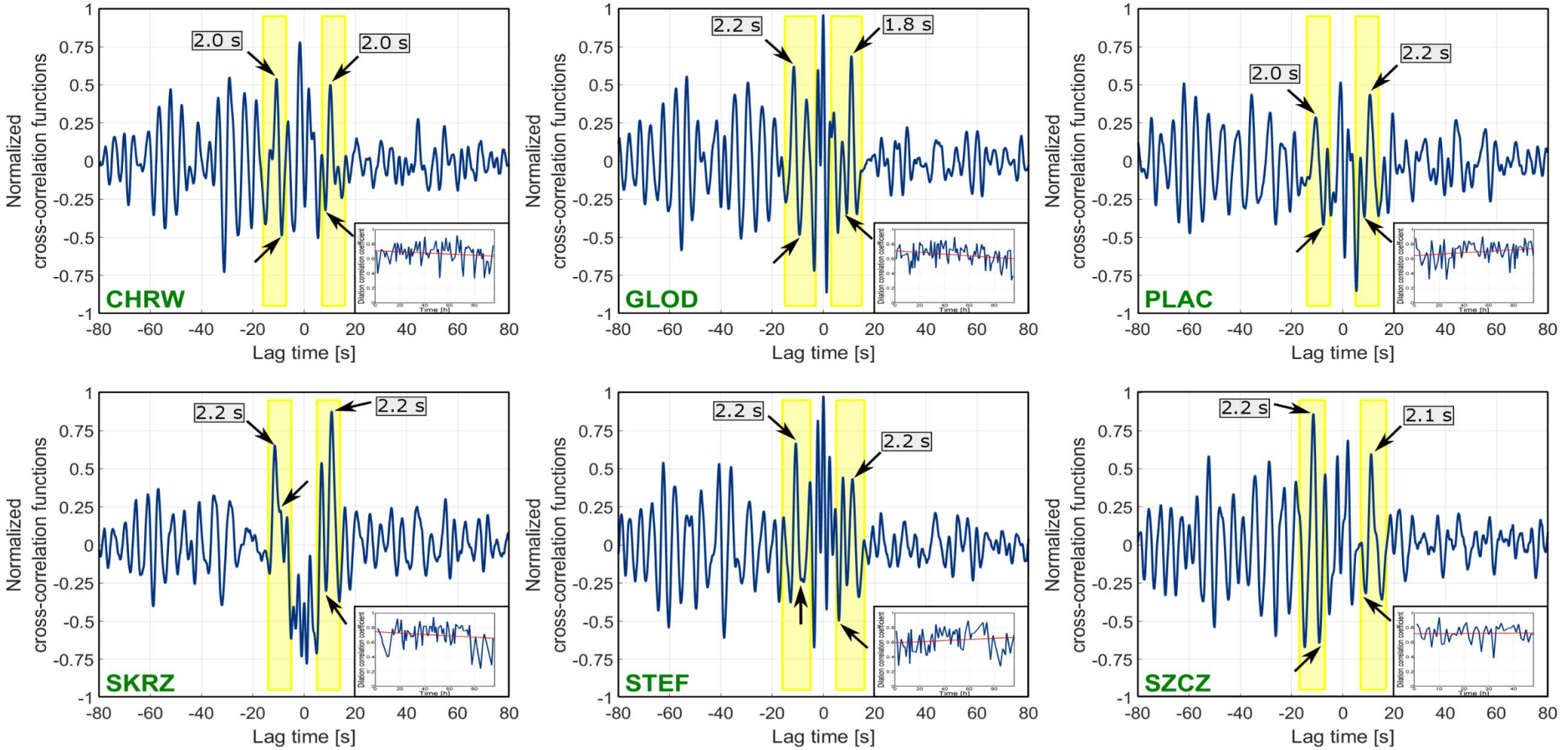


**Fig. 8** The average correlograms calculated for six stations from 1-hour horizontal components of seismic noise records. Stretching parameter calculated in a 5 - 15 sec time window.

**Arrows** - arrival times of faster and slower split shear waves, **square boxes** - differences between arrival times of split waves.

Institute of Geophysics
Polish Academy of Sciences

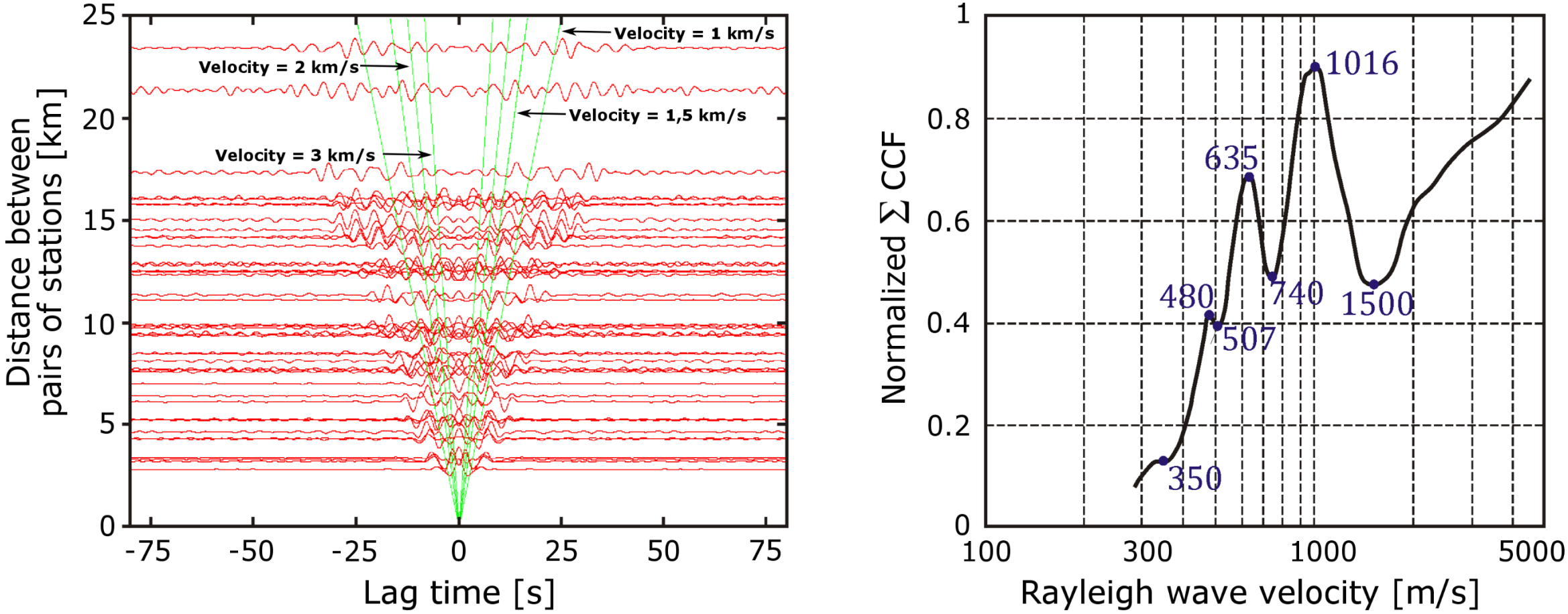


**Fig. 9** The time-distance domain over the whole network, calculated for the cross-correlations of the Z-component of ambient noise, stacked in the period 19.03.2016 – 25.04.2016 and band-pass filtered by the range 0.1 - 0.4 Hz. The green lines indicate the modes of the Rayleigh waves (**left**).

Sum of correlation values obtained by slant-stack in function of Rayleigh wave velocity (**right**). Values are normalized by number of traces.

# Dominant noise frequency band

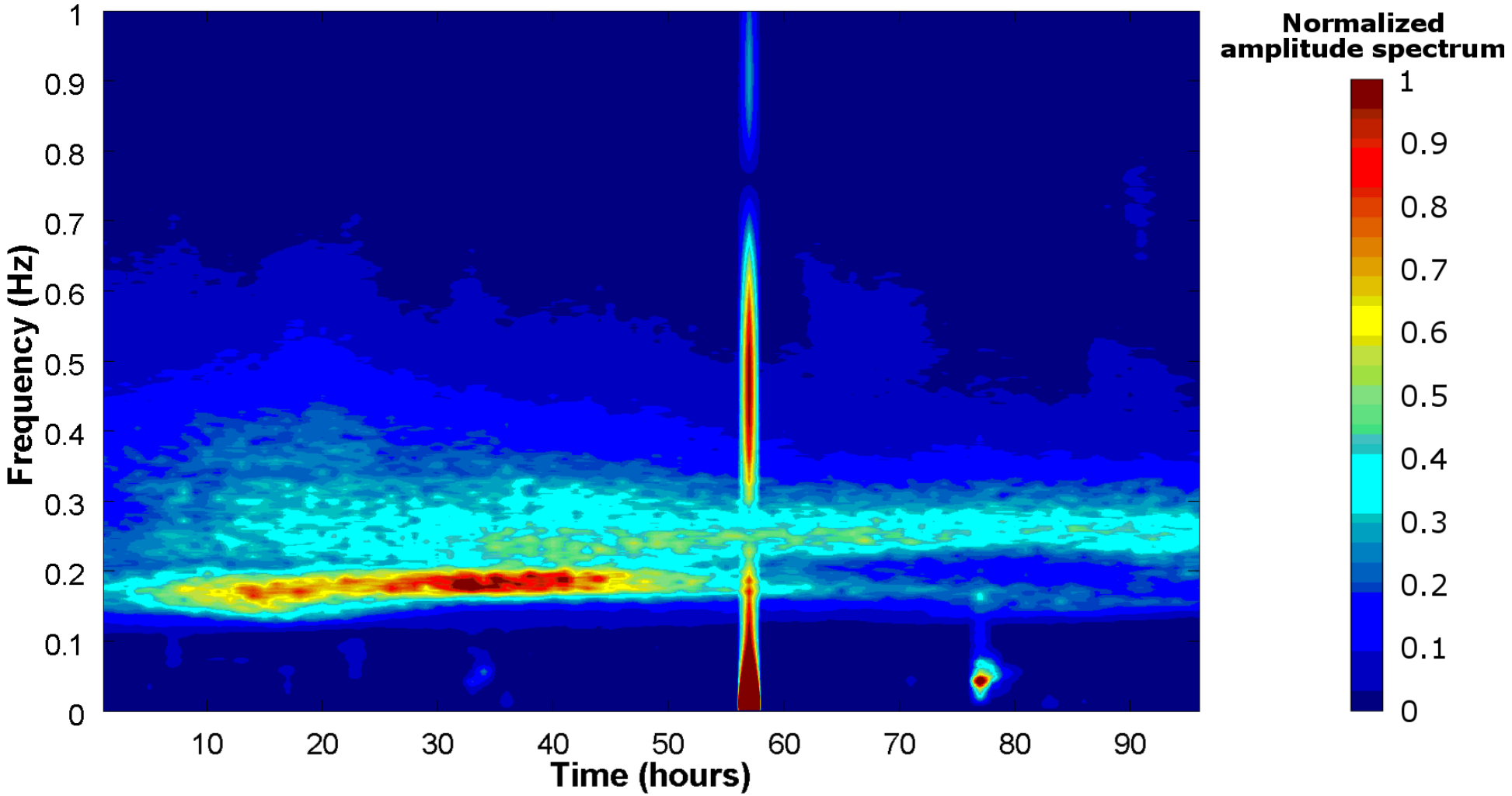


**Fig. 10** Amplitude spectrum of the seismic noise vertical component for PLAC station in a 0 - 1 Hz frequency range; the scale bar represents normalized amplitude spectrum. Spectrum was calculated for the period 1st - 4th November 2015.

# Influence of the local sources on the CCF shape

**Fig. 11** Correlograms calculated from the vertical components of the following noise records:

**Fig. 11a** - The STEF-SZCZ profile (7746 m); the data (19.03.2016 - 25.04.2016) were filtered in the frequency band **0.05 – 2 Hz**,

**Fig. 11b** - The STEF-SZCZ profile (7746 m); the data (19.03.2016 - 25.04.2016) were filtered in the frequency band **0.1 – 0.4 Hz**,

**Fig. 11c** - The average value correlograms presented in Fig. 11a and Fig. 11b.

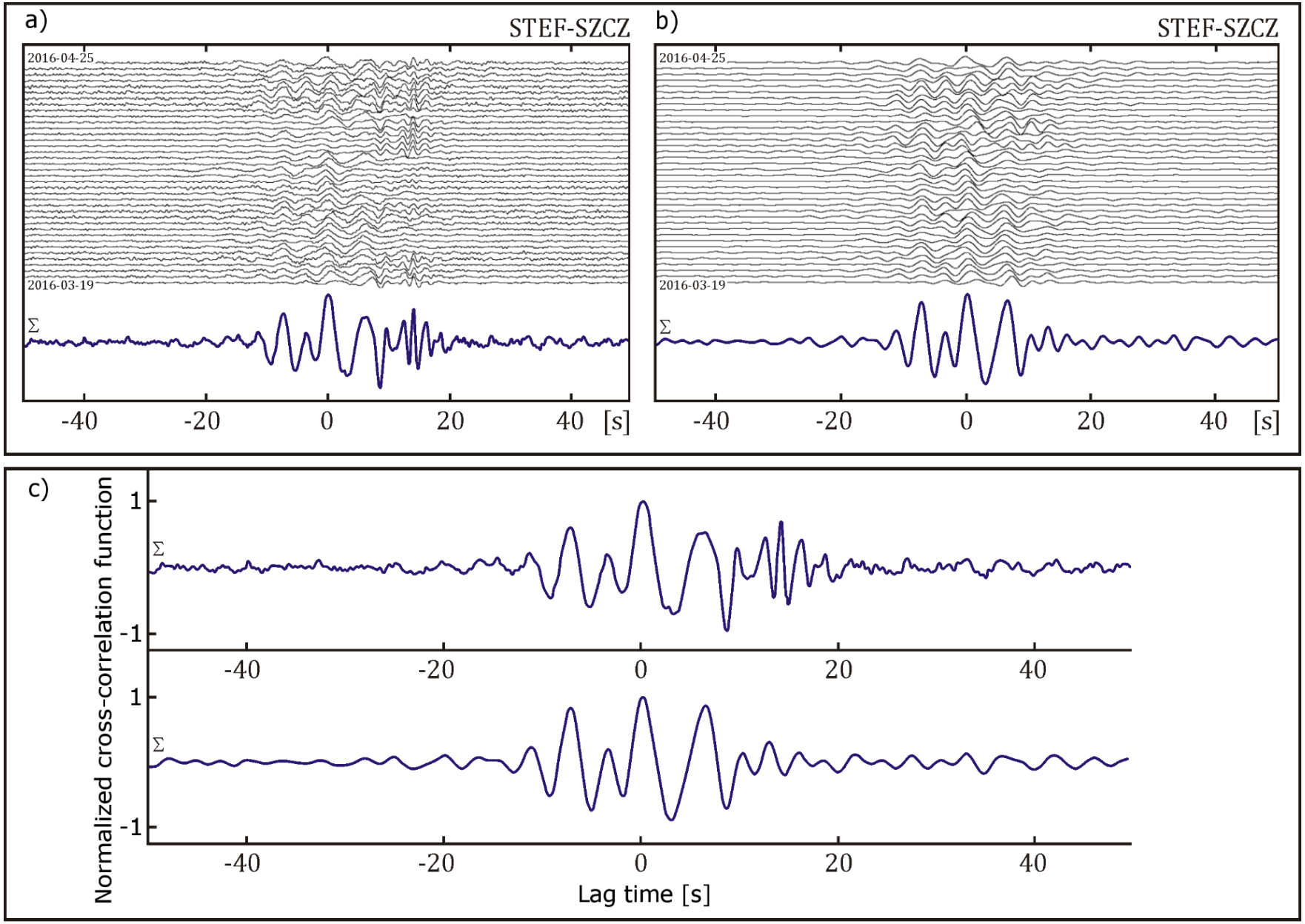


Institute of Geophysics
Polish Academy of Sciences

# Stability of the CCF over longer periods of time

**Fig.12** Correlograms calculated from the vertical components of the following noise records:

**Fig. 12a** - The PLAC-SZCZ profile (7616 m); the data (**01.12.2015 - 31.01.2016**) were filtered in the frequency band 0.1 – 0.4 Hz; red ovals - disturbed signals,

**Fig. 12b** - The PLAC-SZCZ profile (7616 m); the data (**19.03.2016 - 25.04.2016**) were filtered in the frequency band 0.1 - 0.4 Hz,

**Fig. 12c** - The average values correlograms presented in Fig. 12a and Fig. 12b.

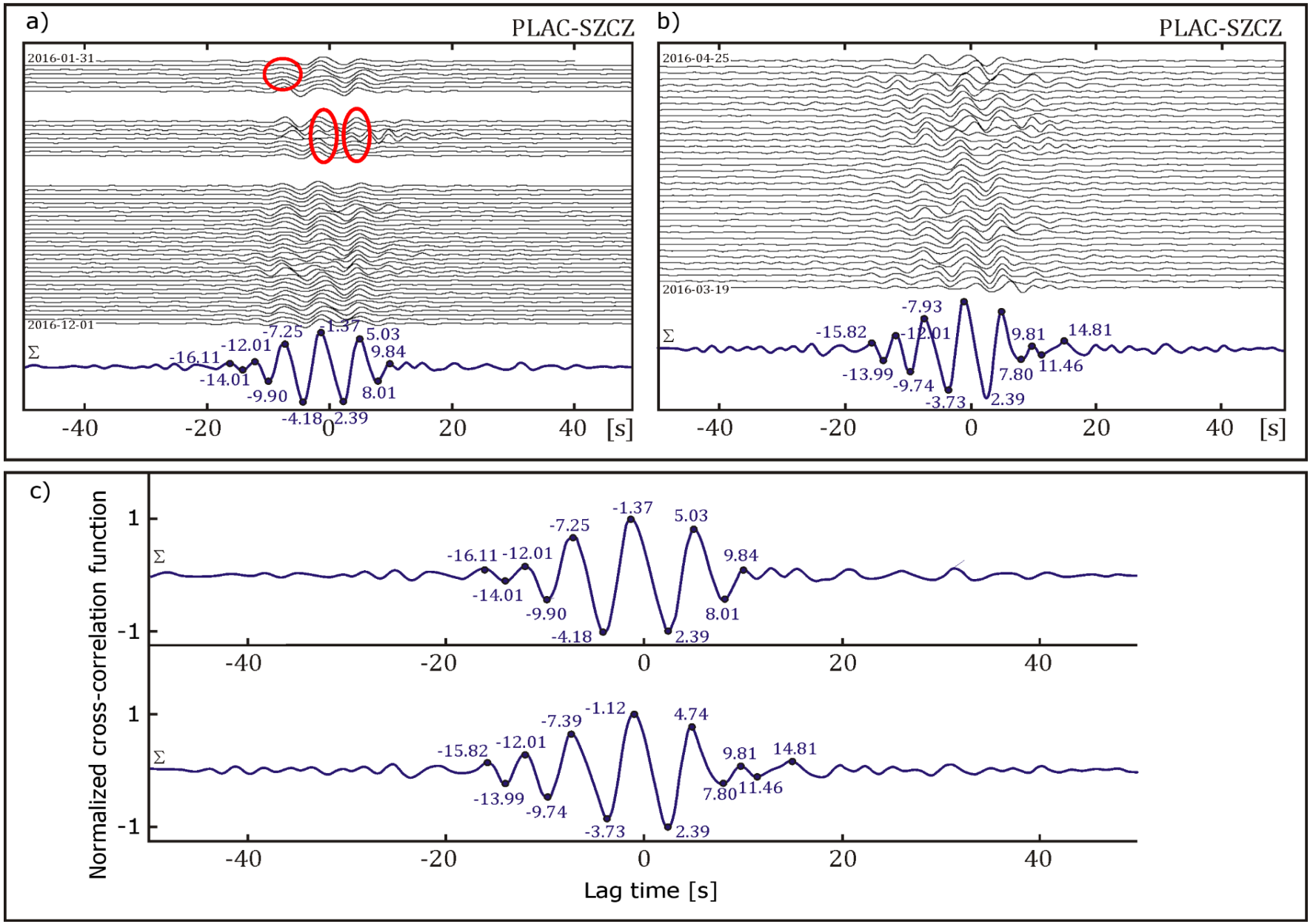


Institute of Geophysics
Polish Academy of Sciences